here. Also, the fields we used are typical of those encountered in CE, and the electrokinetic preconcentration occurring at the entrance of the sieving polymer can lead to high DNA concentrations. We observed that aggregation can occur in a polymer-containing sieving buffer as well as in free solution, if large DNA molecules are present. Thus, aggregation can explain why electrophoregrams present numerous irreproducible peaks (*1*, *2*), because each aggregate passing the detector yields a spurious peak. Understanding how aggregation occurs will be necessary to eliminate or reduce its occurrence and to extend the range of sizes and field strengths presently available for electrophoretic separations in liquid solutions.

REFERENCES AND NOTES

1. P. D. Grossman and J. C. Colburn, Eds., *Capillary Electrophoresis: Theory and Practice* (Academic Press, San Diego, 1992).
2. S. Hjerten, T. Srichaiyo, K. Elenbring, paper presented at High Performance Capillary Electrophoresis '91, San Diego, CA, 3 to 6 February 1991.
3. T. Guszczynski, H. Pulayeva, T. Tietz, M. Garner, A. Chrambach, *Electrophoresis* **14**, 523 (1993).
4. Other concentrations of ethidium bromide were used without qualitative effects on the results.
5. See, for example, (*1*), p. 313.
6. The overlap concentration for T4 and λ DNA is 48 and 86 μg/ml, respectively, evaluated with a persistence length of 500 Å and the Kratky-Porod formula. [O. Kratky and G. Porod, *Recl. Trav. Chim.* **68**, 1106 (1949)].
7. H. A. Pohl, *Dielectrophoresis* (Cambridge Univ. Press, Cambridge, UK, 1978), p. 135.
8. Y. Hu, J. L. Glass, A. E. Griffith, *J. Chem. Phys.* **100**, 4674 (1994).
9. See, for example, M. Jonsson, U. Jacobson, M. Takahashi, B. Norden, *J. Chem. Soc. Faraday Trans.* **89**, 2791 (1993); Z. Wang, R. Xu, B. Chu, *Macromolecules* **23**, 790 (1990). This may also explain why the dielectric constant of DNA solutions is difficult to measure below 10^4 Hz [M. Mandel, *Ann. N.Y. Acad. Sci.* **303**, 74 (1977)].
10. L. Song and M. F. Maestre, *J. Biomol. Struct. Dyn.* **9**, 525 (1991).
11. F. Brochard-Wyart and P. G. de Gennes, *C. R. Acad. Sci. Paris Ser. II* **307**, 1497 (1988).
12. This work was supported by European Community grant 930018 of the Human Genome program. We are indebted to A. Ajdari, H. Isambert, P. Lammert, L. Leibler, M. Rubinstein, G. Weill, and B. Zimm for stimulating discussions and comments.

3 August 1994; accepted 1 November 1994

High-Rate, Gas-Phase Growth of MoS_2 Nested Inorganic Fullerenes and Nanotubes

Y. Feldman, E. Wasserman, D. J. Srolovitz, R. Tenne*

The gas-phase reaction between MoO_{3-x} and H_2S in a reducing atmosphere at elevated temperatures (800° to 950°C) has been used to synthesize large quantities of an almost pure nested inorganic fullerene (IF) phase of MoS_2. A uniform IF phase with a relatively narrow size distribution was obtained. The synthesis of IFs appears to require, in addition to careful control over the growth conditions, a specific turbulent flow regime. The x-ray spectra of the different samples show that, as the average size of the IF decreases, the van der Waals gap along the *c* axis increases, largely because of the strain involved in folding of the lamella. Large quantities of quite uniform nanotubes were obtained under modified preparation conditions.

Although graphite is the most stable form of carbon under ambient conditions, graphite nanoclusters have been shown to be unstable against folding and to close into fullerenes (*1*), nested fullerenes (NFs) (*2*), and nanotubes (*3*). It is believed (*4*) that the main stimulus to form carbon fullerenes (CFs) emanates from the large energy associated with the dangling covalent bonds of the peripheral carbon atoms in graphite nanoclusters. Recent theoretical work (*5*) suggests that multilayer NFs are thermodynamically more stable than single layer fullerenes that have the same number of carbon atoms. Although the growth conditions in most cases are far from equilibrium, some evidence in support of this theoretical work was obtained by careful annealing of amorphous carbon soot with the beam of a transmission electron microscope (TEM) (*6*).

Nanoclusters of layered metal dichalcogenide materials, such as WS_2, were also recently shown (*7–9*) to be unstable against folding and to close on themselves to form NF-like structures (also designated IFs) and nanotubes, which are similar to their carbon predecessors. Although the driving force in this case is not likely to be very different, the detailed structure of the IFs is quite different from that of the CFs, largely because the structures of graphite and layered dichalcogenides are different. In particular, the IFs are generally more faceted than the CFs (*8*, *9*). In both the CFs and IFs, these folded, three-dimensional fullerenes are characterized by topological point defects on the basal planes of the regular crystal structure (*10*). However, the topological defects are much stronger in the IF structures than in the CF structures.

Because CFs can be considered a metastable form of carbon, it was suggested (*11*) that the ideal growth conditions for CFs could be provided through a gas-phase reaction. In this case, each nanocluster is isolated in the reaction chamber, and the only means for it to release its extra energy is through collisions with the noble carrier gas (He in most experiments). Development of a similar strategy for the IFs would be desirable but requires careful consideration and detailed knowledge of the phase equilibria in the reaction chamber.

However, the choice of source materials for a gas-phase reaction is fairly extensive. For example, preparation of MoS_2 powders and films by the gas-phase reaction between $MoCl_x$ (x = 3 to 5) and H_2S (*12*) or MoF_6 and H_2S (*13*) has been demonstrated. Alternatively, pulsed laser evaporation (*14*) and metal organic chemical vapor deposition (*15*) can be used to form IF from the gas phase.

To take advantage of the sublimation of MoO_{3-x} at relatively low temperatures (>650°C), we built a reactor that allowed for a gas-phase reaction between a stream of gaseous molybdenum suboxide and H_2S. This reactor was used to prepare, reproducibly, a few milligrams of an almost pure IF phase in each run. The production of copious amounts of IFs allowed a systematic study of the properties of the IF, the initial results of which are also reported here. Furthermore, the analysis of the growth conditions provided some clues to the pathway of IF production. Minor changes in the reactor design resulted in the production of substantial numbers of nanotubes up to 5 μm in length with diameters of 10 to 20 nm.

To form MoS_2 from H_2S and MoO_3 in a reducing atmosphere at elevated temperatures, the Mo-S-O ternary phase diagram should be considered (*16*) (see the schematic in Fig. 1). The following reactions are relevant for the growth of MoS_2 (represented by arrows in the phase diagram):

$$MoO_3(s) + xH_2(g) \rightarrow MoO_{3-x}(g) + xH_2O(g) \tag{1}$$

$$MoO_{3-x}(g) + (1-x)H_2(g) + 2H_2S(g) \rightarrow MoS_2(s) + (3-x)H_2O(g) \tag{2}$$

$$MoO_3(s) + 3H_2(g) \rightarrow Mo(s) + 3H_2O(g) \tag{3}$$

Y. Feldman and R. Tenne, Department of Materials and Interfaces, Weizmann Institute, Rehovot 76100, Israel.
E. Wasserman, Central Research and Development Laboratories, E. I. du Pont de Nemours, Experimental Station, Wilmington, DE 19898, USA.
D. J. Srolovitz, Department of Materials and Interfaces, Weizmann Institute, Rehovot 76100, Israel, and Department of Materials Science and Engineering, University of Michigan, Ann Arbor, MI 48109, USA.

*To whom correspondence should be addressed.

$$MoO_{3-x}(g) + (1 - x)H_2(g) + xH_2S(g) \rightarrow MoO_{2-x}S_x(s) + H_2O(g) \quad (4)$$

Nonstoichiometry commonly occurs in metal oxides, including the Mo compounds. One may also take advantage of the fact that some of the substoichiometric oxides are very volatile and sublime at temperatures as low as 650°C (reaction 1). However, if the reducing atmosphere is too strong, metallic Mo, which has an exceedingly low vapor pressure at these temperatures (reaction 3), occurs. On the other hand, if the reducing atmosphere in the reactor is not sufficiently strong, oxisulfides of Mo with an orthorhombic structure collect on the substrate (for example, reaction 4). Careful control of the reducing atmosphere in the reaction chamber is a prerequisite for the successful production of the elusive IF phase through reaction 2.

The dominant phase in the Mo-S phase diagram in the low-temperature and excess sulfur regime is the amorphous MoS_3 (a-MoS_3) compound (*13*). At high reaction temperature, 2H-MoS_2 predominates. This situation, which is represented by reactions 5 and 6 on the ternary phase diagram (Fig. 1), is favorable for the growth of IFs, because by losing S the a-MoS_3 phase is expected to slowly transform into nanocrystallites of MoS_2 in the gas phase and spontaneously collapse into IFs (*8*). This growth mechanism was particularly favorable for the growth of IFs through the solid-gas reaction (*7*, *8*). To what extent an amorphous cluster of molybdenum trisulfide or oxisulfide serves as a precursor to IF in the present gas-phase reaction is not clear at this point.

A schematic illustration of the reactor is shown in Fig. 2. In the early design (Fig. 2A) the fluxes of the two gases were not separated and IFs were obtained only sporadically. To obtain IF particles of homogeneous size, we modified the original reactor (Fig. 2B). To separate the gas fluxes, we introduced an additional tube to deliver powdered MoO_3 (*17*). Moreover, the exit of this tube was turned 90° with respect to the main gas stream, and the size and shape of the nozzle were carefully designed. To ensure the appropriate reducing atmosphere in each of the gas streams, two separate sources of forming gas (5% H_2 and 95% N_2) were necessary. The flow of the various gases was automatically controlled. Any small change in the flow regime adversely influenced the reaction products. We found that a turbulent flow regime, which was difficult to control and maintain, yielded the best and most reproducible results. To produce this turbulent regime, we introduced another change into the original chamber, as indicated in Fig. 2. The collecting quartz substrate was put behind a high wall of the boat ~3 cm upstream from the crossing point of the two gases (*18*). The quartz slides with the products were used as such for the x-ray diffraction (XRD) measurements, or the products were transferred onto Cu grids (*19*) for inspection in a TEM.

A series of TEM images from the various

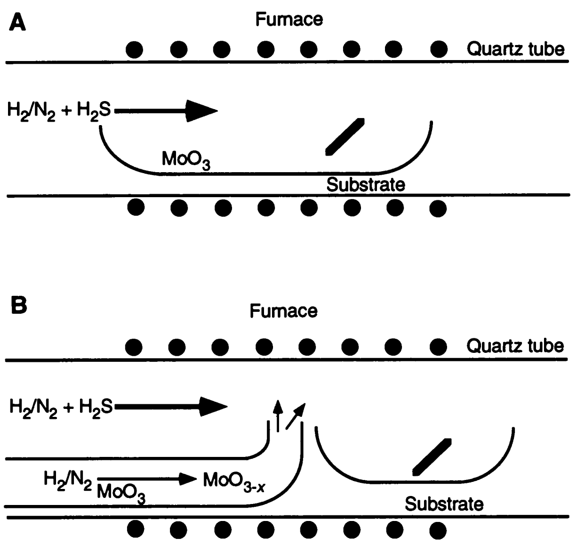

Fig. 2. (**A**) Schematic representation of the early gas-phase reactor used to produce MoS_2 IFs. In the later version (**B**), two separate gas streams were obtained by the introduction of a tube for molybdenum suboxide flow. We obtained a turbulent flow regime by putting the collecting substrate behind a high wall.

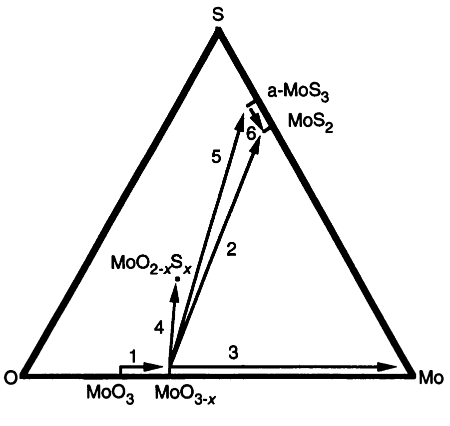

Fig. 1. Ternary phase diagram of Mo-S-O, showing the different routes to obtain MoS_2.

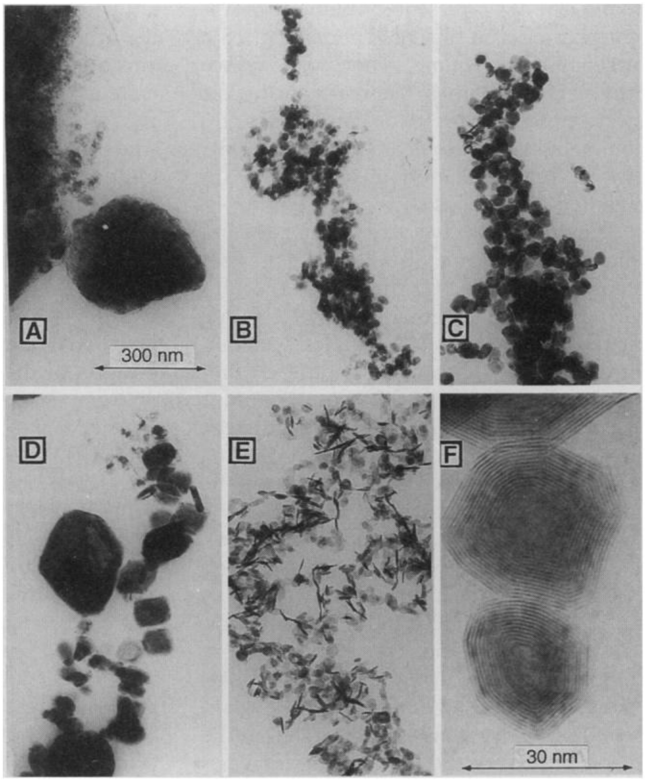

Fig. 3. Series of TEM images showing the structure of IF-MoS_2: (**A**) amorphous phase produced at 800°C; (**B**) IF of 20-nm average size obtained at 820°C; (**C**) IF of 40-nm average size obtained at 840°C; (**D**) mixed IF (100-nm average size) and platelets (100 to 300 nm) obtained at 900°C; (**E**) 2H-MoS_2 phase prepared at 840°C under the laminar flow regime; (**F**) high-magnification image of two typical IFs obtained at 840°C. The distance between each two fringes is $c/2 = 0.62$ nm. The fluxes of the various gases in the reactor are as follows: H_2S, 1.5 cm^3/min; mixture of H_2 (5%) and N_2 (95%), 90 cm^3/min in the main tube and 30 cm^3/min in the inner tube (see Fig. 2B). The Cu grids for the TEM experiments were covered with amyl acetate film to close the gap between the Cu filaments. A 5-nm film of amorphous carbon was deposited on top to render the insulating film conductive.

Table 1. Internal radii *r* (± 0.2 nm) of the hollow cores of IFs with different thicknesses of the spherical shell *h* and number of shells *k*. The upper row is a set of ascending average radii which increase by increments of 0.6 nm. The flow rates in the main sample tube (see Fig. 2B) for a mixture of H_2 (5%) and N_2 (95%) and H_2S were 90 and 1.5 cm^3/min, respectively, for samples a, c, and e; 115 and 1.5 cm^3/min, respectively, for sample d; and 70 and 1.0 cm^3/min, respectively, for sample b. For the inner tube, the flow rate of the mixture of H_2 (5%) and N_2 (95%) was 40 cm^3/min for sample b and 30 cm^3/min for the other samples. The radii are reported in the column of the average radii observed (see text).

k	*h* (nm)	*r* (nm)									
		1.4	2.0	2.6	3.2	3.8	4.4	5.0	5.6	6.2	6.8
3	1.86				3.2^a	3.7^a		4.8^b			
4	2.48			2.6^b	3.2^a						
5	3.10			2.6^c						6.5^b	
6	3.72			2.6^a	3.2^b						
7	4.34		2.1^e							6.0^d	
8	4.96				3.1^a						
9	5.58			2.6^e							7.0^a
10	6.20		2.0^a	2.6^e							
11	6.82	1.5^e		2.6^c					5.6^a		
12	7.44		1.9^a		3.4^e						
13	8.06				3.3^b						
14	8.68		1.9^e			3.9^c					
15	9.30				3.4^b						
16	9.92		2.0^d								
17	10.54										
18	11.16			2.6^b							
19	11.78						4.2^e				

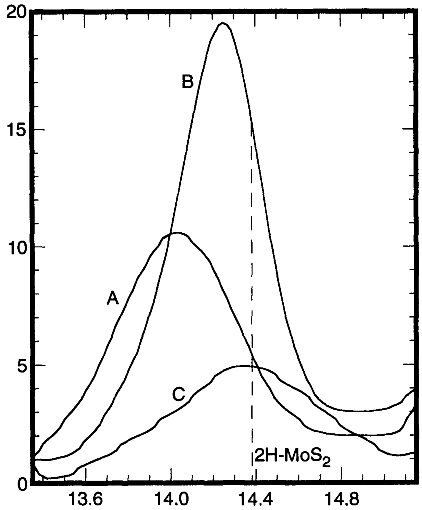

Fig. 4. Powder XRD spectrum taken from the phases obtained during the growth of MoS_2 at 840°C (curve A), 900°C (curve B), and 840°C under laminar flow conditions (curve C).

reaction products, which were obtained at different temperatures, is shown in Fig. 3. For temperatures up to 800°C, an amorphous phase was obtained (Fig. 3A), which yielded a broad peak in XRD spectra and a fuzzy electron diffraction pattern. Growth at 820°C produced IFs ~20 nm in (external) diameter (Fig. 3B). The average size of the IFs increased with increasing reaction temperature. A typical example obtained at 840°C is shown in Fig. 3C. Here the average external diameter is ~40 nm.

When the reaction was allowed to proceed for 2 hours instead of 1 hour, there was no noticeable change in the IF size distribution. This result suggests that the sizes and morphologies of the IFs are determined during growth in the gas phase. It further suggests that the products of the gas-phase reaction were obtained under quasi-equilibrium conditions, so that a theoretical analysis with equilibrium mechanics is warranted (see below).

At a growth temperature of 900°C, the external diameter of the IFs was 100 nm and the wall thickness was ~20 nm (Fig. 3D). Platelets 100 to 300 nm long and longer, belonging to the 2H-MoS_2 polytype, start to appear at this temperature. If the temperature of the reactor is increased further, the fraction of 2H-MoS_2 predominates and becomes the sole phase at 950°C. In this case most of the crystallites were oriented with their ⟨0001⟩ axis perpendicular to the substrate (*20*). Higher annealing temperatures yielded even larger crystallites of the same phase. The IFs represented the most prevalent phase in the film only under a specific turbulent flow regime. They were visible only very rarely in a laminar flow regime even at temperatures (840°C) where IFs predominate in the turbulent flow regime (Fig. 3E). A high-resolution image of two IFs obtained at 840°C is shown in Fig. 3F.

We systematically analyzed the radii and thicknesses of some 110 IFs, which were prepared at 850°C. Of this number, 28 IFs with a spherical internal (hollow) core are reported in Table 1. The samples were taken from a few different batches, each prepared under somewhat different conditions (see the caption of Table 1). The different IFs were arranged according to an ascending thickness *h* of the spherical shell (along the columns) and an ascending radius *r* of the (hollow) core of the IF (along the rows). The innermost layer of the IF is always complete, and the value of *h* increases by 0.6 nm, which is ~*c*/2, along the columns. This result shows that the IFs are made of complete layers and not of patches of 2H-MoS_2 "glued" together through grain boundaries. The analysis also shows that the average radius of the hollow core increases also by 0.6 nm along the rows from the smallest radius observed, 1.4 nm. A still smaller inner radius of 0.8 nm cannot be excluded, although it has not been observed. This result suggests that well-defined steric criteria determine the structure of the innermost layer of the IFs.

The spacing between two adjacent layers in CFs (*c*/2) and nanotubes was somewhat larger than that of bulk graphite (*21*). The lattice expansion was ascribed to strain relief in the folded structure. A similar mechanism for strain relief was expected to operate in the IFs. A series of XRD spectra for the various films prepared on quartz substrates is shown in Fig. 4. The scattering intensity of the thin films was very weak, and therefore lengthy measurements were taken for each film. TEM measurements taken before and after each of the runs confirmed that the morphology of the species did not change during the long (15-hour) XRD experiments. The (0002) peak position in the XRD pattern depended not only on temperature but also on the flow regime, as expected from the TEM results. The XRD pattern for the film prepared in the turbulent flow regime at temperatures between 800° and 900°C corresponded to that of the IF phase seen in TEM. The sample prepared at 840°C showed an average expansion of 2% along the *c* axis (Fig. 4, curve A) compared with the 2H phase (vertical line). The average size of the crystallites was calculated from the Debye-Scherrer formula to be 40 nm (see also Fig. 3C). Upon increasing the temperature to 900°C (Fig. 4, curve B), the intensity of the peak increased and the shift from the peak position of the 2H phase decreased (see also Fig. 3D). The average size of the crystallites was 100 nm at this temperature, which suggests a reduced strain for the larger IF. The XRD spectrum of the specimen obtained within the laminar flow regime (Fig. 4, curve C) at 840°C (see also Fig. 3E) corresponded to the 2H bulk phase. The low intensity and the large width of the peak suggested that the crystallites were very small. TEM observations showed that these crystallites were in the form of small platelets (15 nm). The XRD spectra of the samples that were heated to

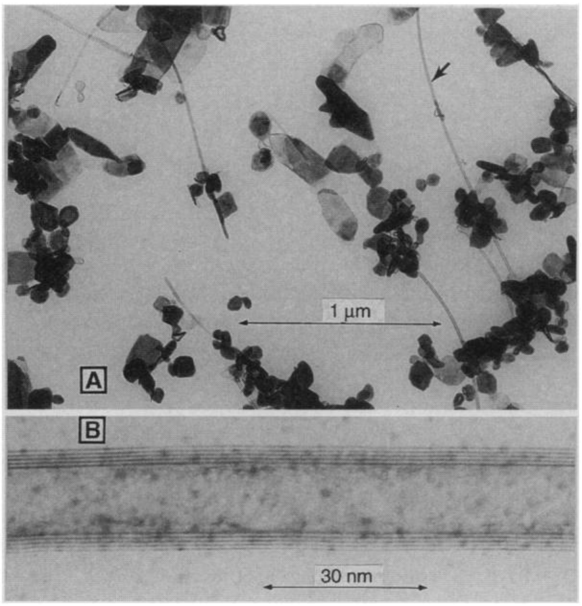

Fig. 5. (**A**) Assortment of nanotubes obtained by the gas-phase reaction of MoO_{3-x} and H_2S in a reducing atmosphere at 850°C. (**B**) High-magnification image of the arrowed tube in (A). The distance between each two fringes is $c/2$ = 0.62 nm.

≥950°C corresponded to the bulk 2H phase, independent of the flow regime. The XRD results were consistent with the TEM observations and confirmed the growth of the IF phase. Both the TEM and XRD results confirmed the importance of the turbulent flow regime for the production of the IF phase. The increased van der Waals gap ($c/2$) of the IF suggests an easier intercalation of small alkali ions into the IF compared with the bulk 2H polytype.

When the nozzle of the exit gas mixture containing MoO_{3-x} was made very narrow, substantial quantities of nanotubes were obtained (see Fig. 5A). These nanotubes were very uniform in shape (Fig. 5B): most of them contained between 5 and 10 layers of MoS_2, and their lengths exceeded a few micrometers. In fact, many of the nanotubes were cut during the transfer process onto the Cu grid. The nanotubes were mixed with a separate phase consisting of 2H-MoS_2 platelets. This process allows a reproducible production of copious numbers of nanotubes, although still not as the major constituent as in the case of IF.

A few indications suggest that the need for a turbulent flow regime is not unique to the present system. In fact, the arc-discharge method, which was devised for the production of large quantities of CF (*22*), nanotubes (*23*), or metal carbohedrenes (*24*), is not maintained under laminar flow conditions. In this case, the hot plasma produced near the electrodes is likely to be turbulent, but in contrast to the present method, the transition from laminar to turbulent flow conditions cannot be controlled. A turbulent flow regime is likely to produce better mixing of the reacting gases in the growth chamber and hence increase the rate of reactions in the growth chamber.

The growth mechanism of NFs of both carbon and MoS_2 is not yet fully understood. It is quite clear that the IF phase is produced in the gas phase of the reactor. Therefore, the role of the quartz substrate is only that of a collector. Recent calculations (*25*), based on continuum elastic theory and surface energetics, indicate that, in thermodynamic equilibrium, the ratio of the NF radius (R) to their thickness, $R/h = r/h + 1/2$, is independent of the size of the NF. Thus, one expects that, when the temperature is increased so that larger NFs are produced, the NF should also become thicker so that R/h remains constant. The present experiments clearly indicate that as R increases so does h, but R/h is not necessarily constant.

It is possible that the kinetic barriers are too high for the IF phase to be in a real equilibrium state. The continuum theory also suggests that NFs are metastable with respect to particles of the bulk phase. The presence of thick NFs may be attributable to their thermodynamic stability as single- or double-layer fullerenes followed by subsequent growth on the surfaces of these small nuclei. However, the faster kinetics and larger thermal energies available at the higher growth temperature allow for more complete equilibration of the growing material, and hence particles belonging to the 2H polytype would be kinetically (and thermodynamically) preferred over thick NFs. Also, it is likely that an internal pressure develops in the hollow core of the IF as a result of the imprisoned carrier gas. This internal pressure weakens the bonds in the point defects of the closed shell, leading finally to a breakdown of the IF at elevated temperatures.

REFERENCES AND NOTES

1. H. W. Kroto, J. R. O'Brien, J. R. Heath, R. F. Curl, R. E. Smalley, *Nature* **318**, 162 (1985).
2. S. Iijima, *J. Cryst. Growth* **50**, 675 (1980).
3. ———, *Nature* **354**, 56 (1991).
4. D. H. Robertson, D. W. Brenner, C. T. White, *J. Phys. Chem.* **96**, 6133 (1992).
5. A. Maiti, C. J. Brabec, J. Bernholc, *Phys. Rev. Lett.* **70**, 3023 (1993); J. P. Lu and W. Yang, *Phys. Rev. B* **49**, 11421 (1994).
6. D. Ugarte, *Nature* **359**, 707 (1992); *Europhys. Lett.* **22**, 45 (1993).
7. R. Tenne, L. Margulis, M. Genut, G. Hodes, *Nature* **360**, 444 (1992).
8. L. Margulis, G. Salitra, R. Tenne, M. Talianker, *ibid.* **365**, 113 (1993).
9. M. Hershfinkel *et al.*, *J. Am. Chem. Soc.* **116**, 1914 (1994).
10. H. Kroto, *Science* **242**, 1139 (1988).
11. Q. L. Zhang *et al.*, *J. Phys. Chem.* **90**, 525 (1986); H. W. Kroto, *Nature* **329**, 529 (1987).
12. H. Arctowski, *Z. Anorg. Allg. Chem.* **8**, 213 (1895); P. R. Bonneau, R. F. Jarvis Jr., R. B. Kaner, *Nature* **349**, 510 (1991); N. Imanishi, K. Kanamura, Z. Takehara, *J. Electrochem. Soc.* **139**, 2082 (1992).
13. E. Furimsky and C. H. Amberg, *Can. J. Chem.* **53**, 3567 (1975); W. L. Lee, T. M. Besmann, M. W. Stott, *J. Mater. Res.* **9**, 1474 (1994).
14. M. S. Donley, N. T. McDevitt, T. W. Hass, P. T. Murray, J. T. Grant, *Thin Solid Films* **168**, 335 (1989).
15. W. K. Hofmann, *J. Mater. Sci.* **23**, 3981 (1988).
16. Hydrogen was considered here as a reducing agent only. However, hydrogen is known to intercalate into MoO_3 [see, for example, S. P. Mehandru and A. B. Anderson, *J. Am. Chem. Soc.* **110**, 2061 (1988)].
17. We noticed that, if the oven is turned off overnight, oxisulfides are produced in the next run, probably because of the absorption of water on the quartz.
18. A strong indication of the necessity of the turbulent flow regime was the fact that in this case the IF film was found to cover both sides of the quartz slide. When we used the laminar flow regime, only the forward face was covered with a film. The color of the IF film was brown, that of the amorphous film was yellow, and that of the polycrystalline film was metallic gray.
19. The Cu grids were first covered with amyl acetate to block the holes, and then a thin film (10 nm) of amorphous carbon was evaporated on top to render the area conductive.
20. Typically, metal dichalcogenide films adopt this morphology when grown at these elevated temperatures. See, for example, G. Salitra, G. Hodes, E. Klein, R. Tenne, *Thin Solid Films* **245**, 180 (1994).
21. Y. Saito, T. Yoshikawa, S. Bandow, M. Tomita, *Phys. Rev. B* **48**, 1907 (1993); Y. Yosida, *Appl. Phys. Lett.* **64**, 3048 (1994); M. Li and J. M. Cowley, *Ultramicroscopy* **53**, 333 (1994).
22. W. A. Krätschmer, L. D. Lamb, K. Fostiropoulos, D. R. Huffman, *Nature* **347**, 354 (1990).
23. T. W. Ebbesen and P. M. Ajayan, *ibid.* **358**, 220 (1992).
24. S. F. Cartier, Z. Y. Chen, G. J. Walder, C. R. Sleppy, A. W. Castleman Jr., *Science* **260**, 195 (1993).
25. D. J. Srolovitz, S. A. Safran, R. Tenne, *Phys. Rev. B* **49**, 5260 (1994).
26. We are grateful to S. Safran, G. Hodes, L. Margulis, M. Homyonfer, V. Lyakhovitskaya, and Y. Rosenberg for illuminating discussions. D.J.S. gratefully acknowledges the hospitality of the Weizmann Institute of Science. The research of D.J.S. was supported in part by the Michael Visiting Professorship and the Division of Materials Science of the Office of Basic Energy Sciences of the U.S. Department of Energy (grant FG02-88ER-45367). The research of R.T. was supported by the U.S.–Israel Binational Science Foundation (grant 94-11-002) and the Israeli Ministry of Energy and Infrastructure (grant 92-00175).

23 August 1994; accepted 31 October 1994